

Original Article

Accuracy in Non-linear Frequency Estimate of an Euler-Bernoulli Beam with Strong Geometric Non-Linearity using First Order and Second-Order Perturbation Methods

Suresh N Shankaranarayana¹, Chandrashekhara C V²

^{1,2} Department of Mechanical Engineering, PES University, Bengaluru, Karnataka, India.

¹nssuresh70@gmail.com

Received: 07 March 2022

Revised: 07 May 2022

Accepted: 11 May 2022

Published: 31 May 2022

Abstract - The ability to accurately estimate the non-linear frequency and response of general mechanical structures and beams is critical for their dynamic design. In the present study, the non-linear dynamics of the beam system is investigated using first-order and second-order perturbation techniques. The boundary conditions of pinned-pinned, clamped-clamped, and clamped-pinned ends are explored. The results from the two techniques are compared with the frequency from the exact solution and response from Runge-Kutta 4th order solution. The ratio of non-linear frequency to linear frequency is studied and demonstrated that the ratio increases with the increasing initial deflection and decreasing beam thickness. It is demonstrated that the error with the first-order frequency estimate, as compared with the exact solution, increases with the increasing non-linear frequency ratio.

In contrast, the error with the second-order technique reduces with the increasing non-linear frequency ratio. For the given system configuration, the absolute error percentage from both techniques appears to cross over around a non-linear frequency ratio of about 1.8. The response from the first and second-order techniques matches closely with the Runge-Kutta solution in moderate and strong non-linear regimes, respectively.

Keywords - Non-linear vibration, Euler-Bernoulli beam, mid-plane stretch, perturbation technique, free vibration

1. Introduction

In engineering, an understanding of the dynamic characteristics of systems and equipment is critical in ensuring their safe and reliable operation in service. Failure of many mechanical systems is attributed to issues caused by vibration, from simple wear to catastrophic failures of rotating systems. In reality, most systems behave non-linearly. Non-linearity can be caused by many different factors such as material properties, geometric non-linearity, external forces and constraints, free-play, backlash, impact, and friction [1]. Beam, a fundamental element, is used in most analysis work, including non-linear behavior. Non-linear analyses of the vibrating systems are more rigorous and complex. Studying the non-linear nature of vibration of its constituent variables and responses is important in understanding and applying it accurately in engineering. Due to the complex nature of the mathematical model, exact solutions to non-linear problems are few. Most models depend on approximate analytical models to understand the system response.

2. Literature Review

Numerous studies have been conducted on arriving at approximate analytical solutions for the vibration of beams under geometric non-linearity, using various methods. Rao and Pillai [2] investigated the free vibrations with large deflection of simply supported beams. Several approaches are applied to solve the equation of motion, such as the perturbation technique, harmonic balance (HMB), Galerkin method, etc. They concluded that the results from the second approximation of HMB compared to the exact solution match well. Lestari and Hanagud [3] investigated buckled beams' linear and non-linear vibrational characteristics with immovable boundary conditions (BC). They used Jacobi elliptic functions to arrive at the non-linear solution of the beam vibration. They opined that axial load and amplitude affect beams with stiffer end constraints to a lesser degree. When the axial compressive load is equal to the crippling load, the non-linear frequency varies linearly with amplitude. Ahmadian et al. [4] applied the homotopy perturbation (HPM) and modified Lindstedt-



Poincare methods to investigate the non-linear vibration of beams with midplane stretch. They demonstrated that the response matches with numerical methods. They performed a parametric study on various slenderness ratios and axial loads. Peng et al. [5] developed a semi-analytical technique for non-linear vibration analysis of Euler-Bernoulli (EB) beams with geometric non-linearity. They investigated perturbation, differential quadrature, and time-domain expansion methods. They compared with numerical results, which showed accuracy and convergence characteristics. Xinmou et al. [6] obtained the analytical solutions for the non-linear vibration of the electromagnetically excited cantilever using HPM. They compared numerical results and concluded that the method provides an accurate solution with first-order approximation. Sedighi et al. [7] solved the governing equation of non-linear vibration of the cantilever using six analytical methods. They compared numerical results and concluded that single-term expansion provides accurate solutions. Barari et al. [8] investigated the responses of a clamped-clamped buckled beam for the first mode by variational iteration and parametrized perturbation. They showed that the frequency obtained by both methods is the same and compares well solution from Runge-Kutta 4th order (RK4) technique. Das et al. [9] performed the numerical analysis of beams with different BCs under large amplitude with free and forced excitations. They used the Hamiltonian approach (HA) to obtain the governing equation and variational form of energy principle for the static problem. They determined system stiffness using static deflection and used the same stiffness to solve the free vibration problem. They presented the numerical results, which matched with available literature. Jafari et al. [10] solved the non-linear vibration of EB beams by using the differential transform method (DTM), two auxiliary parameters for the homotopy analysis method (HAM). They compared the solution with numerical results and demonstrated that the results matched. Bagheri et al. [11] used methods of He's variational technique and the Laplace iteration to explore the non-linear responses of a fixed beam. The results are compared with the RK4 solution, and concluded that the results are extendable to other non-linear vibrations. Pakar and Bayat [12] used He's a variational technique to get a solution for the non-linear vibrations of the axially loaded EB supported beam. They showed that the method applies to a wide range of initial amplitudes. The solution obtained is compared with the numerical solution and found to be accurate. Azimi and Kariman [13] investigated the non-linear vibration of an axially loaded EB beam using HA and DTM to solve for natural frequency as a function of initial deflection. The illustrative examples shown are compared with the exact solution. Motallebi et al. [14] used HAM to find the non-linear vibratory behavior of a pinned-pinned beam, formulating the system as a quintic equation. They showed that the Homotopy-Pade technique leads to a reduced number of approximations for a given accuracy. They parametrically studied the effects of

variations of the axial load and slenderness ratio on beam behavior. They concluded that HAM is an accurate and powerful technique for solving non-linear beam equations. Barry [15] investigated the first five modes in the non-linear vibration of the beam due to mid-plane stretch, subject to axial loads, and supporting many rigid bodies. He validated the analytical model by employing the finite element approach and compared the results to those found in the literature. He demonstrated a shift of non-linearity to softening type when an axial load is introduced, using numerical simulations. Mohammadrezazadeh et al. [16] used HAM and Homotopy Pade technique to perform a parametric vibration study on a clamped-clamped beam with axial load and lateral harmonic excitation. They concluded that lower computational efforts are required to execute HAM and Homotopy Pade techniques, and second-order approximation provides accurate results. Ding et al. [17] studied non-linear beam vibration considering the effect of asymmetry in its elastic supports. They employed the multiple scales method to investigate the transformation of characteristics from hardening type from softening type, resulting from geometric non-linearity and asymmetry in BCs, which is valid in the first mode. Dang and Le [18] investigated the non-linear vibration of compressively loaded EB beam on an elastic foundation using equivalent linearization and weighted averages. They compared the results with He's variational approach and the RK4 solution and demonstrated the accuracy of the used approach. Effects of Winkler elastic foundation coefficient and compressive force were investigated. Friis et al. [19] established linear dynamic systems with multiple degrees of freedom equivalent to non-linear systems, using energy dissipation methods and least-squares fit. They conducted numerical Ansys trials to demonstrate the methods provide a reliable estimate for various engineering structures. Bayat et al. [20] used Improved Amplitude Frequency Formulation to investigate the railway track system under axial loading. They modeled the system using the Winkler spring approach to represent the soil condition and Euler Bernoulli beam approximation to extract the fundamental frequencies of the system. They ran a sensitivity analysis that considered the effects of axial loads and soil stiffnesses. They concluded that the first iteration of the method produces an accurate result. Rincon-Casado et al. [21] studied the effect of the BCs on the free non-linear frequency and variation concerning the beam's amplitude. They deployed analytical and numerical methods. They arrived at the analytical solutions using non-linear normal modes and multiple scales approaches. Using Abaqus software, the results are compared to a non-linear FE model. Loghman et al. [22] investigated the non-linear dynamic characteristics of fractional visco-elastic micro-beam. Using the Hamilton principle, they used the von-Karman strain and Kelvin-Voigt model to model the beam. The finite difference method, Galerkin's method, and Shooting methods were used for the solution. They showed that the order of the

fractional derivative is high when the amplitude is high and when the excitation frequency is closer to the resonant frequency. Outassafte [23] et al. studied the linear and non-linear vibration of a circular arch which is inextensible and has ends constrained in rotation. They used the Euler-Bernoulli formulation with Von Karman strains inducing geometric non-linearity. They discretized the total strain energy, solved the resulting non-linear equations numerically using the approximate method, and arrived at backbone curves depicting frequency dependence on amplitude. Lacarbonara and Yabuno [24] used the geometrically exact theory of rods to investigate the extensible or inextensible hinged beams. They obtained closed-form solutions using the multiple scales method and Mettler model and compared them with results from the literature. They obtained backbone curves for a given geometric configuration and compared them with experimental results for the first mode. The experimental results matched the analytical prediction. Hu [25] used the classical perturbation technique to arrive at an approximation of non-linear frequency for strong nonlinearities. He solved the Duffing equation using the second-order non-linear parameter in assumed solutions of non-linear frequency and response to arrive at an approximation of frequency and response for large values of non-linear coefficient. He showed that the solution works well for small or large values of non-linear coefficients. He estimated the maximum error in non-linear frequency, compared to the exact solution, to be less than 0.03%.

The mathematical solution of a beam's non-linear dynamic behavior is a developing field with numerous attempted approaches. There is scope to improve the available techniques and applicability of different techniques for different geometric configurations. The present paper reports the solution for the strong geometric non-linearity of an Euler-Bernoulli beam using two approaches. Three boundary conditions (BCs) investigated are pinned-pinned (PP), clamped-clamped (CC), and clamped-pinned (CP) types. Classical first-order and second-order perturbation techniques investigate the accuracy of predicting non-linear frequency and response for a slender beam under strong geometric non-linearity.

3. Mathematical Model

The Present work considers an Euler-Bernoulli beam system with immovable supports, as shown in Figure 1. Immovable supports result in the mid-plane stretch during vibration. The slender beam of cross-sectional area A_b , length l , the moment of inertia I , mass density ρ , and Young's modulus E is used for the mathematical modeling. Three BCs of PP, CC, and CP are considered.

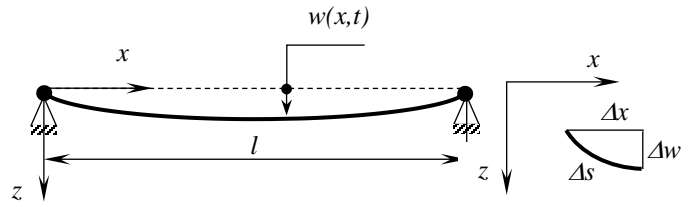


Fig. 1 Axial stretching of a beam with immovable supports

3.1. Equation of Motion of the Beam

The beam's instantaneous transverse deflection at a distance x from one end at time t is given by $w(x, t)$. The governing non-linear partial differential equation (PDE) of the beam, without an axial load and a forcing function, under the influence of mid-plane stretch, is given by [1].

$$EI \frac{\partial^4 w}{\partial x^4} - \frac{EA_b}{2l} \int_0^l \left(\frac{\partial w}{\partial x}\right)^2 dx \frac{\partial^2 w}{\partial x^2} + \rho A_b \frac{\partial^2 w}{\partial t^2} = 0 \quad (1)$$

The governing equation is decomposed into ordinary differential equations using Galerkin's approach. Solution $w(x, t)$ from Equation 1 is assumed to be,

$$w(x, t) = \sum_{j=1}^N \phi_j(x) q_j(t) \quad (2)$$

Spatial and temporal dimensions of the transverse deflection $w(x, t)$ are separated in Equation 2, where $\phi_j(x)$ for the j^{th} mode represents the beam's linear undamped normal vibrational mode and $q_j(t)$ represents the beam's corresponding modal coordinate.

Substituting Equation 2 into Equation 1, PDE is transformed to ordinary differential equation given by,

$$\sum_{j=1}^N EI \frac{d^4 \phi_j}{dx^4} q_j - \frac{EA_b}{2l} \sum_{j=1}^N \sum_{k=1}^N \sum_{l=1}^N \int_0^l \left(\frac{d\phi_k}{dx} q_k\right) \left(\frac{d\phi_l}{dx} q_l\right) dx \frac{d^2 \phi_j}{dx^2} q_j + \sum_{j=1}^N \rho A_b \phi_j \ddot{q}_j = 0 \quad (3)$$

where normal mode-shapes are represented by ϕ_j , ϕ_k , and ϕ_l , and modal coordinates are represented by q_j , q_k , and q_l . "When applying the Galerkin method to non-linear terms, each approximation of w needs to have a separate set of indices, to ensure that all possible modal cross-coupling terms are captured in the model" [1] and hence indices k & l are introduced. Linear terms are decoupled by multiplying and integrating Equation 3 by an arbitrary mode ϕ_n .

$$\sum_{j=1}^N EI \int_0^l \phi_n \frac{d^4 \phi_j}{dx^4} q_j dx - \frac{EA_b}{2l} \sum_{j=1}^N \sum_{k=1}^N \sum_{l=1}^N \int_0^l \phi_n \int_0^l \left(\frac{d\phi_k}{dx} q_k\right) \left(\frac{d\phi_l}{dx} q_l\right) dx \frac{d^2 \phi_j}{dx^2} q_j dx + \sum_{j=1}^N \int_0^l \phi_n \rho A_b \phi_j \ddot{q}_j dx = 0 \tag{4}$$

The mode shapes considered in the analysis do not have axial loads. Equation 4 is simplified using orthogonality conditions and integrals of standard mode shapes. The following sections simplify Equation 4 for three different boundary conditions.

3.1.1. Pinned-Pinned Boundary Condition

The beam with pinned-pinned BC is shown in Figure 2.

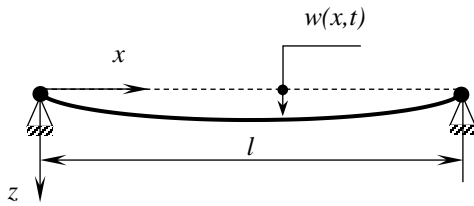


Fig. 2 Axial stretching of a pinned-pinned (PP) beam

The linear undamped natural frequency for a beam with pinned-pinned boundary condition, ω_{nj} for the j^{th} mode, is given by,

$$\omega_{nj} = (\beta_j l)^2 \sqrt{\frac{EI}{\rho A_b l^4}} \tag{5}$$

where $\beta_j l = j\pi$;

The corresponding mode shape is given by,

$$\phi_j(x) = \sin\left(j\pi \frac{x}{l}\right) \tag{6}$$

Equation 4 is solved to get the equation of motion for the pinned-pinned boundary condition [1]:

$$\ddot{q}_j(t) + \omega_{nj}^2 q_j(t) + \sum_{k=1}^N \frac{Ek^2 j^2 \pi^4}{4\rho l^4} q_k^2 q_j = 0 \tag{7}$$

where $j, k = 1, 2, 3 \dots N$;

Equation 7 reduces to the form of Duffing equation for the fundamental mode ($j, k=1$). Suffixes are ignored for simplicity and the equation of motion given by

$$\ddot{q} + \omega_n^2 q + \alpha q^3 = 0 \tag{8}$$

where $\alpha = \frac{E\pi^4}{4\rho l^4}$ for PP beam

3.1.2. Clamped-Clamped Boundary Condition

The beam with clamped-clamped BC is shown in Figure 3.

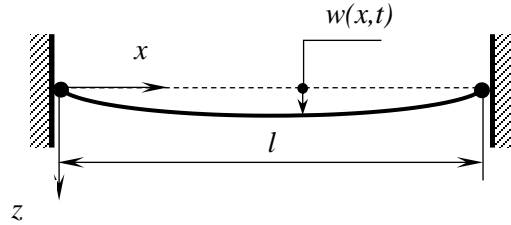


Fig. 3 Axial stretching of a clamped-clamped (CC) beam

The linear undamped natural frequency for a beam with clamped-clamped boundary condition, ω_{nj} for the j^{th} mode, is given by,

$$\omega_{nj} = (\beta_j l)^2 \sqrt{\frac{EI}{\rho A_b l^4}} \tag{9}$$

where $\beta_1 l = 4.7300$; $\beta_2 l = 7.8532$ etc.

The corresponding mode shape is given by [26],

$$\phi_j(x) = \{\cos(\beta_j x) - \cosh(\beta_j x)\} - \sigma_j \{\sin(\beta_j x) - \sinh(\beta_j x)\} \tag{10}$$

where $\sigma_j = \frac{\cos(\beta_j l) - \cosh(\beta_j l)}{\sin(\beta_j l) - \sinh(\beta_j l)}$

Using orthogonality conditions, integrals of mode shapes for clamped-clamped beam are given by [27],

$$\int_0^l \left(\frac{d\phi_k}{dx}\right) \left(\frac{d\phi_l}{dx}\right) dx = K_1 = \sigma_j \beta_j (\sigma_j \beta_j l - 2) \text{ for } l = k \text{ or } 0 \text{ if } l \neq k \tag{11}$$

$$\int_0^l \phi_n \phi_j dx = l \text{ for } j = n \text{ or } 0 \text{ if } j \neq n \tag{12}$$

$$\int_0^l \phi_n \phi_j'''' dx = \beta_j^4 l \text{ for } j = n \text{ or } 0 \text{ if } j \neq n \tag{13}$$

$$\int_0^l \phi_n \left(\frac{d^2 \phi_j}{dx^2}\right) dx = K_2 = \sigma_j \beta_j (1 - \sigma_j \beta_j l) \text{ for } j = n \text{ or } 0 \text{ if } j \neq n \tag{14}$$

The Equation 11 to 14 are substituted into each term in Equation 4, solved and simplified to obtain expression for each term as,

$$\sum_{j=1}^N EI \int_0^l \phi_n \frac{d^4 \phi_j}{dx^4} q_j dx = \sum_{j=1}^N (\rho A_b l) \omega_{nj}^2 q_j \tag{15}$$

$$\begin{aligned} & \frac{EA_b}{2l} \sum_{j=1}^N \sum_{k=1}^N \sum_{l=1}^N \int_0^l \phi_n \int_0^l \left(\frac{d\phi_k}{dx} q_k \right) \left(\frac{d\phi_l}{dx} q_l \right) dx \frac{d^2 \phi_j}{dx^2} q_j dx \\ & = \frac{EA_b}{2l} \sum_{j=1}^N K_1 K_2 \sum_{k=1}^N q_k^2 q_j \end{aligned} \tag{16}$$

$$\sum_{j=1}^N \int_0^l \phi_n \rho A_b \phi_j \ddot{q}_j = \sum_{j=1}^N (\rho A_b l) \ddot{q}_j \tag{17}$$

Substituting Equation 15 to 17 into Equation 4 and simplifying, the equation of motion for CC boundary condition is obtained as,

$$\ddot{q}_j(t) + \omega_{nj}^2 q_j(t) - \sum_{k=1}^N \frac{EK_1 K_2}{2\rho l^2} q_k^2 q_j = 0 \tag{18}$$

where $K_1 = \sigma_j \beta_j (\sigma_j \beta_j l - 2)$ and $K_2 = \sigma_j \beta_j (1 - \sigma_j \beta_j l)$

Equation 18 reduces to the form of Duffing equation for the fundamental mode ($j, k=1$) as given by,

$$\ddot{q} + \omega_n^2 q + \alpha q^3 = 0 \tag{19}$$

where $\alpha = -\frac{EK_1 K_2}{2\rho l^2}$ for CC beam

3.1.3. Clamped-Pinned Boundary Condition

The beam with clamped-pinned BC is shown in Figure 4.

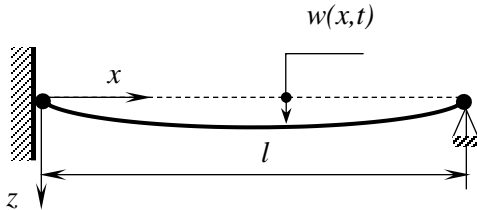


Fig. 4 Axial stretching of a clamped-pinned (CP) beam

The linear undamped natural frequency for a beam with clamped-clamped boundary condition, ω_{nj} for the j^{th} mode, is given by,

$$\omega_{nj} = (\beta_j l)^2 \sqrt{\frac{EI}{\rho A_b l^4}} \tag{20}$$

where $\beta_1 l = 3.9266$; $\beta_2 l = 7.0685$ etc

The corresponding mode shape is given by [26],

$$\phi_j(x) = \{ \cos(\beta_j x) - \cosh(\beta_j x) \} - \sigma_j \{ \sin(\beta_j x) - \sinh(\beta_j x) \} \tag{21}$$

where $\sigma_j = \frac{\cos(\beta_j l) - \cosh(\beta_j l)}{\sin(\beta_j l) - \sinh(\beta_j l)}$

Using orthogonality conditions, the integral of mode shapes for the clamped-clamped beam is given by [27],

$$\begin{aligned} \int_0^l \left(\frac{d\phi_k}{dx} \right) \left(\frac{d\phi_l}{dx} \right) dx & = K_1 = \sigma_j \beta_j (\sigma_j \beta_j l - 1) \text{ for } l \\ & = k \text{ or } 0 \text{ if } l \neq k \end{aligned} \tag{22}$$

Other integrals of mode shapes remain the same as Equations 12 to 14.

Substituting the integrals of mode shapes and simplifying, the equation of motion for CP boundary conditions is obtained as,

$$\ddot{q}_j(t) + \omega_{nj}^2 q_j(t) - \sum_{k=1}^N \frac{EK_1 K_2}{2\rho l^2} q_k^2 q_j = 0 \tag{23}$$

where $K_1 = \sigma_j \beta_j (\sigma_j \beta_j l - 1)$ and $K_2 = \sigma_j \beta_j (1 - \sigma_j \beta_j l)$

Equation 23 reduces to the form of Duffing equation for the fundamental mode ($j, k=1$) as given by,

$$\ddot{q} + \omega_n^2 q + \alpha q^3 = 0 \tag{24}$$

where $\alpha = -\frac{EK_1 K_2}{2\rho l^2}$ for CP beam

3.2. First Order Approximate Solution

Using the classical perturbation technique, the solutions of non-linear frequency ω and response $q(t)$ are assumed as functions of the first linear term in α as

$$\omega^2 = \omega_n^2 + \alpha \omega_1 \tag{25}$$

$$q(t) = q_0(t) + \alpha q_1(t) \tag{26}$$

where ω_1 is an unknown constant, a function of amplitude A and $q_1(t)$ is a displacement function. Initial

conditions at $t=0$ are assumed as $q_0(0) = A_0$ and $\dot{q}_0(0) = 0$; $q_1(0) = 0 = \dot{q}_1(0)$.

Substituting Equations 25 and 26 into Duffing Equation 8,

$$\ddot{q}_0 + \alpha \dot{q}_1 + [\omega^2 - \alpha \omega_1][q_0 + \alpha q_1] + \alpha[q_0 + \alpha q_1]^3 = 0 \tag{27}$$

Expanding and simplifying,

$$(\ddot{q}_0 + \omega_0^2 q_0)\alpha^0 + (\dot{q}_1 + \omega^2 q_1 - \omega_1 q_0 + q_0^3)\alpha + (-\omega_1 q_1 + 3q_1 q_0^2)\alpha^2 + (3q_1^2 q_0)\alpha^3 + (q_1^3)\alpha^4 = 0 \tag{28}$$

Equating the coefficients of 0^{th} and 1^{st} power of α to zero and ignoring coefficients of higher powers of α ,

$$\ddot{q}_0 + \omega^2 q_0 = 0 \tag{29}$$

$$\dot{q}_1 + \omega^2 q_1 = -q_0^3 + \omega_1 q_0 \tag{30}$$

Solution of Equation 29 is given by

$$q_0(t) = A \sin(\omega t + \phi) \tag{31}$$

where ϕ is the phase, the angle

Substituting Equation 31 into Equation 30,

$$\dot{q}_1 + \omega^2 q_1 = -[A \sin(\omega t + \phi)]^3 + \omega_1 [A \sin(\omega t + \phi)] \tag{32}$$

Upon expanding the cubic sine function,

$$\dot{q}_1 + \omega^2 q_1 = -\frac{3}{4}A^3 \sin(\omega t + \phi) + \frac{1}{4}A^3 \sin 3(\omega t + \phi) + \omega_1 A \sin(\omega t + \phi) \tag{33}$$

The first and the last term of RHS lead to secular terms resulting in an unbounded solution. The secular terms are eliminated by taking ω_1 as a function of A .

$$\omega_1 = \frac{3}{4}A^2, \text{ where } A \neq 0 \tag{34}$$

Substituting Equation 34 into Equation 33,

$$\dot{q}_1 + \omega^2 q_1 = \frac{1}{4}A^3 \sin 3(\omega t + \phi) \tag{35}$$

Equation 35 is a standard differential equation whose solution is given by,

$$q_1(t) = B \sin(\omega t + \phi) - \frac{A^3}{32\omega^2} \sin 3(\omega t + \phi) \tag{36}$$

where ϕ is the phase angle

Applying the initial conditions of $q(0) = A_0$ and $\dot{q}(0) = 0$ to Equation 31 yields,

$$A = A_0 \text{ and } \phi = \frac{\pi}{2} \tag{37}$$

Applying initial conditions $q_1 = 0 = \dot{q}_1(0)$ on Equation 36,

$$q_1(0) = 0 = B \sin(\phi) - \frac{A^3}{32\omega^2} \sin 3\phi \tag{38}$$

$$\dot{q}_1(0) = 0 = B\omega \cos \phi - \frac{A^3}{32\omega^2} (3\omega) \cos 3\phi \tag{39}$$

Substituting Equation 37 into Equation 38 and 39 yields,

$$B = -\left(\frac{A^3}{32\omega^2}\right) \text{ and } \phi = \frac{\pi}{2} \tag{40}$$

Substituting the evaluated constants into Equation 36,

$$q_1(t) = \frac{A_0^3}{32\omega^2} (\cos(3\omega t) - \cos(\omega t)) \tag{41}$$

Substituting the evaluated constants and terms into Equation 25 and 26, non-linear frequency and response are obtained as,

$$\omega^2 = \omega_n^2 + \frac{3}{4}\alpha A_0^2 \tag{42}$$

$$q(t) = A_0 \cos(\omega t) + \frac{\alpha A_0^3}{32\omega^2} (\cos(3\omega t) - \cos(\omega t)) \tag{43}$$

It may be noted that Equations 42 and 43 are the same equation used and arrived at by many researchers using various methods, such as by Ahmadian et al. [4], Barari et al. [8], etc.

3.3. Second Order Approximate Solution

Using the classical perturbation technique, Hu [23] obtained the solutions for non-linear frequency ω and response $q(t)$ using second-order approximation.

Non-linear frequency and response are assumed as functions of the second-order term in α as given by

$$\omega^2 = \omega_n^2 + \alpha \omega_1 + \alpha^2 \omega_2 \tag{44}$$

$$q(t) = q_0(t) + \alpha q_1(t) + \alpha^2 q_2(t) \tag{45}$$

Substituting Equation 44 and 45 into Equation 8, expanding,

equating the coefficients of powers on either side, the following results are obtained.

$$\ddot{q}_0 + \omega^2 q_0 = 0 \tag{46}$$

$$\ddot{q}_1 + \omega^2 q_1 = \omega_1 q_0 - q_0^3 \tag{47}$$

$$\ddot{q}_2 + \omega^2 q_2 = \omega_2 q_0 + \omega_1 q_1 - 3q_0^2 q_1. \tag{48}$$

where $\omega_1, \omega_2, q_1(t)$, and $q_2(t)$ are functions of amplitude A and α . The initial conditions are assumed as

$$q_0(0) = A_0 \text{ and } \dot{q}_0(0) = 0; \quad q_i(0) = 0 = \dot{q}_i(0) \text{ for } i \geq 1 \tag{49}$$

Solving the set of equations using the boundary conditions and eliminating secular terms, the second approximate solution to Duffing Equation 8 is obtained. The second-order approximate solution to vibratory response is determined as [23]

$$q(t) = A_0 \cos(\omega t) + \frac{\alpha A_0^3}{32\omega^2} (\cos 3\omega t - \cos \omega t) + \frac{\alpha^2 A_0^5}{1024\omega^4} (\cos 5\omega t - \cos \omega t) \tag{50}$$

with the non-linear frequency given by

$$\omega^2 = \omega_n^2 + \frac{3}{4} \alpha A_0^2 - \frac{3\alpha^2 A_0^4}{128\omega^2} \tag{51}$$

Or, upon simplification,

$$\omega = \frac{1}{4} \sqrt{8\omega_n^2 + 6\alpha A_0^2 + \sqrt{64\omega_n^2 + 96\omega_n^2 \alpha A_0^2 + 30\alpha^2 A_0^4}} \tag{52}$$

3.4. Exact Solution

The non-linear frequencies obtained by the two methods mentioned above are compared against the exact non-linear frequency given by [18]

$$\omega_{ex} = \frac{\pi}{2\sqrt{2}} \left(\int_0^{\pi/2} \left(\frac{d\theta}{\sqrt{2\omega_n^2 + \alpha A_0^2 (1 + \cos^2 \theta)}} \right) \right)^{-1} \tag{53}$$

The results of applying the first approximate solution and second approximate solution and comparing them with an exact solution are provided in the next section.

4. Results and Discussion

Dynamic characteristics of an Euler-Bernoulli beam with a strong geometric non-linearity using first and second-

order methods are extracted. Both methods' accuracy in predicting the natural frequency and response are compared and reported. The geometric parameters and the relevant material properties of the beam used for demonstration are indicated in Table 1.

Table 1. Geometric parameters and material properties of the beam

Description	Notation	Value	Units
Overall length	L	1000	mm
Beam Thickness	t	2 to 10	mm
Beam Width	b	50	mm
Material	-	Steel	-
Young's Modulus	E	2.0×10^{11}	N/m ²
Mass Density	ρ	7850	kg/m ³

Three boundary conditions are considered for the analysis. The coefficient of the non-linear term, α , is estimated for the three BCs, and the values are provided in Table 2.

Table 2. Coefficient of non-linear term α

Boundary Condition (BC)	α	Value in m ⁻² s ⁻²
Pinned-Pinned (PP)	$\frac{E\pi^4}{4\rho l^4}$	6.2044×10^8
Clamped-Clamped (CC)	$-\frac{EK_1 K_2}{2\rho l^2}$	2.6562×10^9
Clamped- Pinned (CP)	$-\frac{EK_1 K_2}{2\rho l^2}$	1.6883×10^9

The thickness of the beam is varied in 2 mm increments from 2 mm to 10 mm. The linear natural frequency of the beam ω_n is evaluated using Equations 5, 9, and 20, respectively, and is tabulated in Table 3.

Table 3. Linear Natural Frequency ω_n in rad/s

Thickness (mm) / BC	PP	CC	CP
2	28.762	65.199	44.931
4	57.524	130.398	89.863
6	86.286	195.597	134.795
8	115.048	260.797	179.726
10	143.81	325.996	224.658

4.1. Non-Linear Frequency using First Approximate Method

The ratio of non-linear frequency (ω) to linear frequency (ω_n), hereafter referred to as NL frequency ratio (ω/ω_n), is estimated using Equation 42 for initial deflection A_0 varying from 0 to 10 mm. The NL frequency ratio is considered a measure of the strength of non-linearity. The graph depicting the NL frequency ratio v/s deflection variation for the three boundary conditions is shown in Figures 5, 6, and 7, respectively.

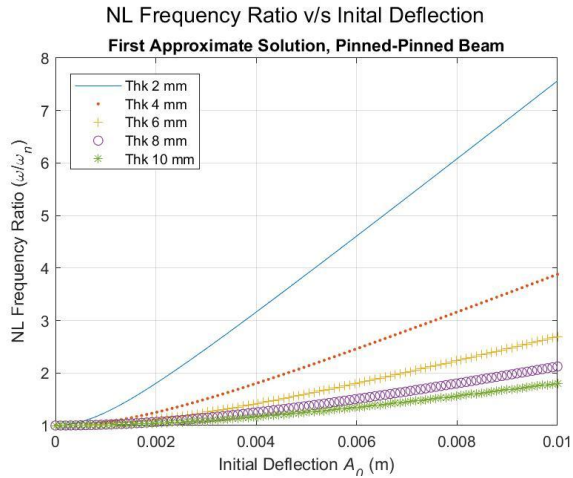


Fig. 5 NL frequency ratio v/s initial deflection for pinned-pinned BC

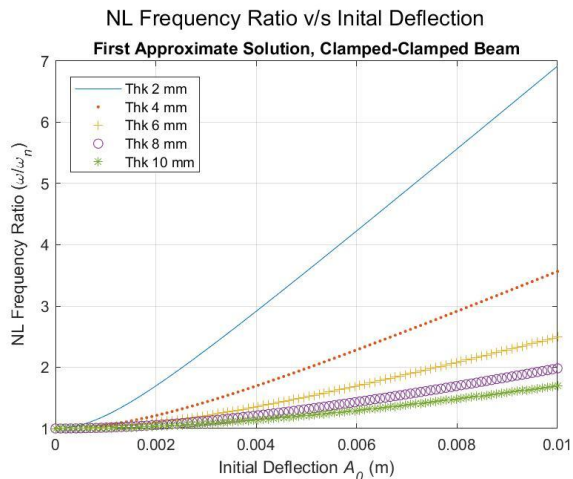


Fig. 6 NL frequency ratio v/s initial deflection for clamped-clamped BC

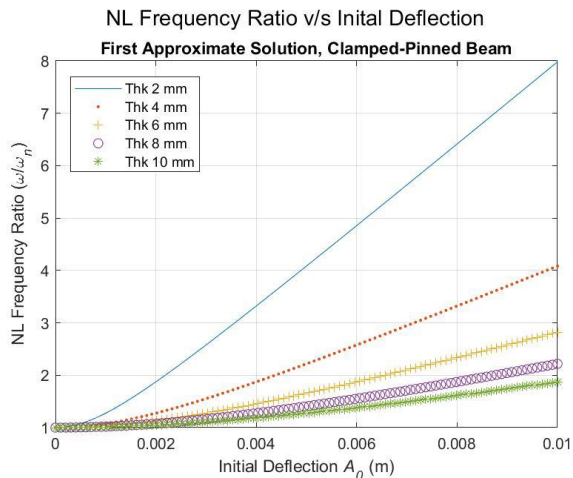


Fig. 7 NL frequency ratio v/s initial deflection for clamped-pinned BC

It is noticed that the value of the NL frequency ratio increases gradually with an increase in initial deflection.

The slope of increase in the NL frequency ratio reduces with an increase in beam thickness. The increase in frequency ratio is gradual and of lesser magnitude with a 10 mm thick beam when compared to a more rapid and higher magnitude of increase in frequency ratio for a 2 mm thick beam. Even though all thicknesses have the same value, the thicker beam has a higher linear frequency, which reduces the frequency ratio for a given deflection. The frequency ratios indicate the magnitude of non-linearity in the problem considered. The behavior of non-linear frequency is in good agreement with the published literature. At zero deflection, the NL frequency ratio attains a value of unity for all boundary conditions, indicating the absence of non-linearity. The NL frequency ratios of 7.41, 6.77, and 7.81, respectively, for *PP*, *CC*, and *CP* beams with 2 mm thickness at maximum initial deflection reduces to 1.78, 1.68, and 1.85, respectively, for 10 mm thick beams.

4.2. Non-Linear Response using First Approximate Method

Mid-point response of the beam by the first approximate method using Equation 43 for an initial deflection of 10 mm is extracted. The plots are generated for two bounding cases of non-linearity, i.e., for a 2 mm thick beam representing strongest non-linearity and a 10 mm thick beam representing moderate non-linearity. Data is extracted in the mid-range for a 6 mm thick beam, and the values are provided in Tables 4 and 5.

Figure 8 shows the mid-point response for pinned-pinned boundary conditions for a 2 mm thick beam and is overlapped with the solution obtained by numerical integration by the Runge-Kutta method of 4th order (*RK4*) for comparison. Figure 9 shows the mid-point response for a 10 mm thick beam.

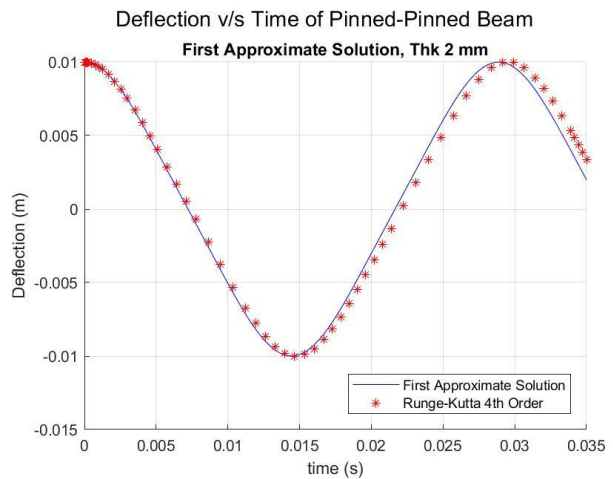


Fig. 8 Mid-point response of 2 mm thick *PP* beam

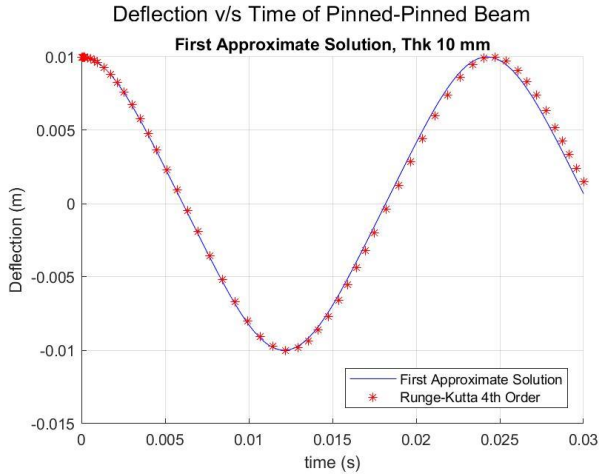


Fig. 9 Mid-point response of 10 mm thick PP beam

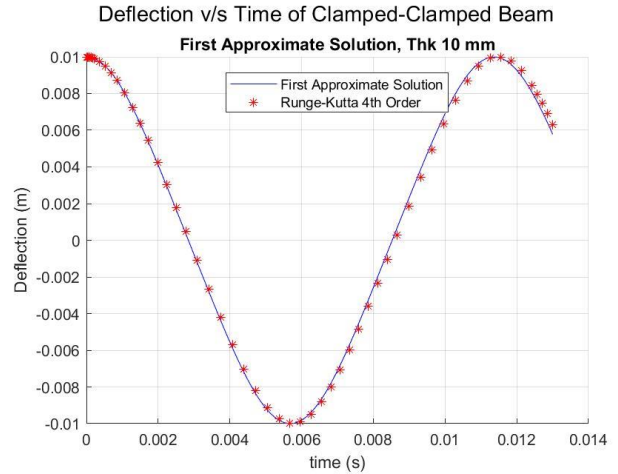


Fig. 11 Mid-point response of 10 mm thick CC beam

Similarly, the behavior of clamped-clamped and clamped-pinned beams is investigated. Figure 10 shows the mid-point response for clamped-clamped boundary conditions for a 2 mm thick beam and is overlapped with the *RK4* solution for comparison. Figure 11 shows the mid-point response for a 10 mm thick beam.

Figure 12 shows the mid-point response for clamped-pinned boundary conditions for a 2 mm thick beam and is overlapped with the *RK4* solution for comparison. Figure 13 shows the mid-point response for a 10 mm thick beam.

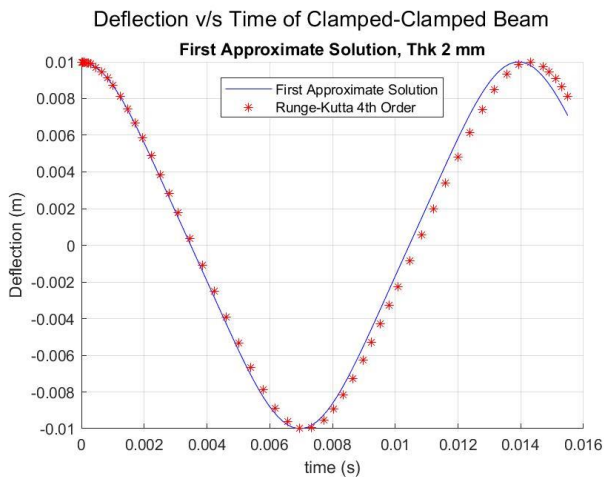


Fig. 10 Mid-point response of 2 mm thick CC beam

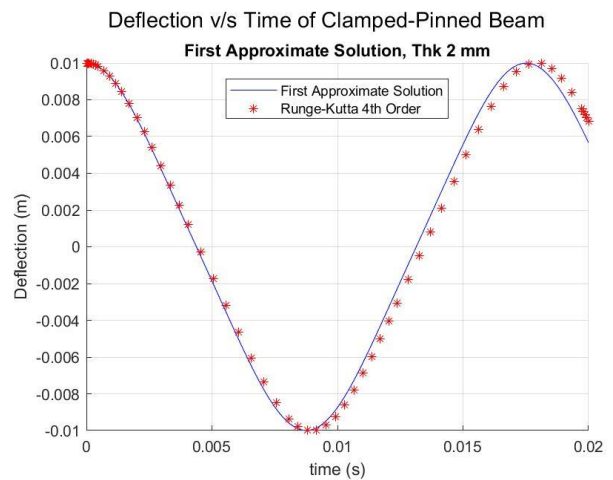


Fig. 12 Mid-point response of 2 mm thick CP beam

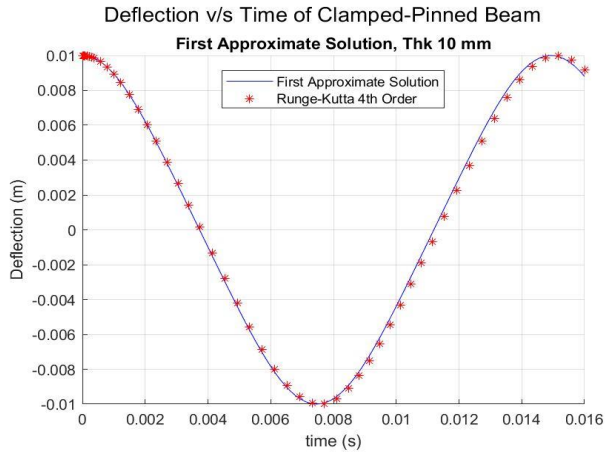


Fig. 13 Mid-point response of 10 mm thick CP beam

The results indicate that the response more closely matches the response from the *RK4* solution for a 10 mm thick beam. A significant variation is found in the case of response from a 2 mm thick beam. The results follow the same pattern for all three boundary conditions. It is noted that the first-order approximate method provides a reasonably accurate response when non-linearity is moderate. In contrast, the response is less accurate in the case of strong nonlinearities.

4.3. Non-Linear Response using Second Approximate Method

The analysis is carried out using the second approximate method. The beam's mid-point response using Equation 50 for an initial deflection of 10 mm is extracted and shown in Figures 14 to 19 for the three boundary conditions of pinned-pinned, clamped-clamped, and clamped-pinned, respectively. The response overlapped with the *RK4* solution for comparison.

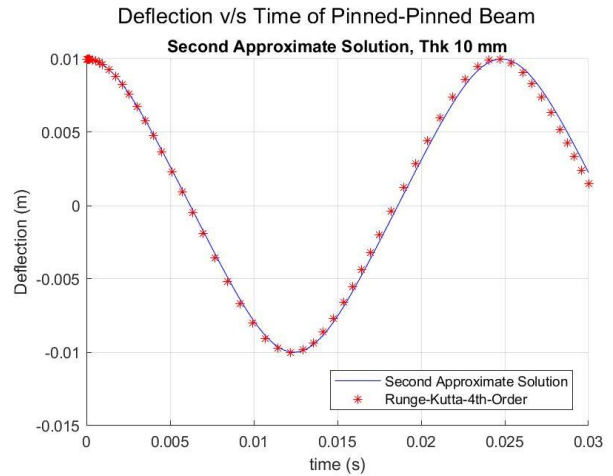


Fig. 15 Mid-point response of 10 mm thick PP beam

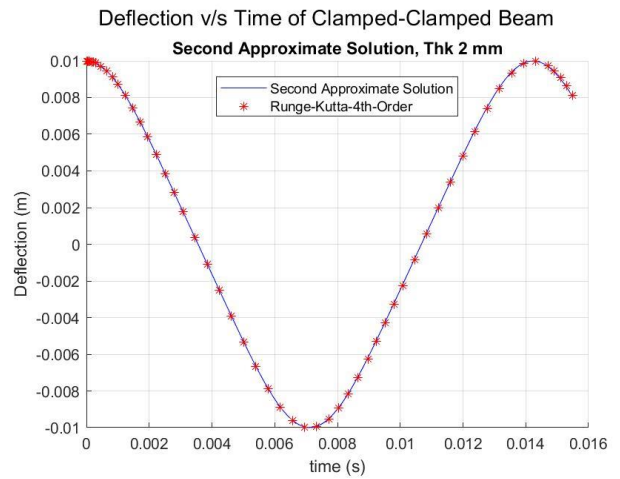


Fig. 16 Mid-point response of 2 mm thick CC beam

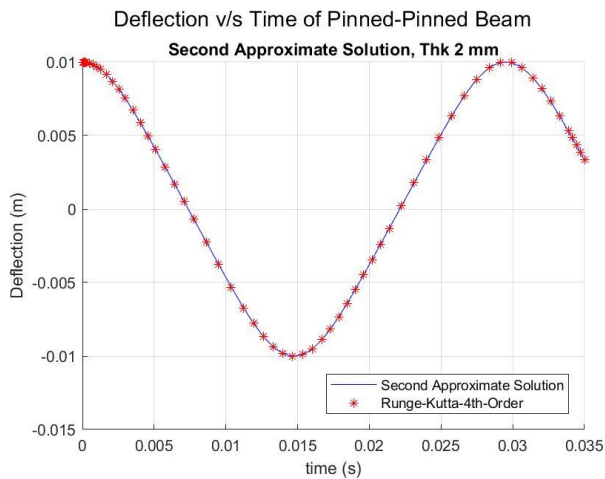


Fig. 14 Mid-point response of 2 mm thick PP beam

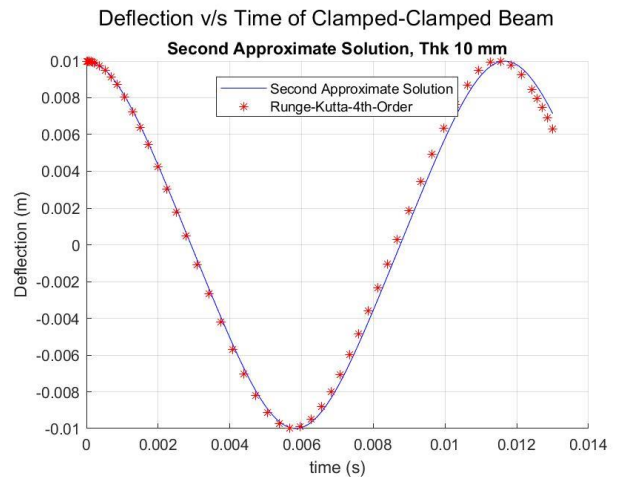


Fig. 17 Mid-point response of 10 mm thick CC beam

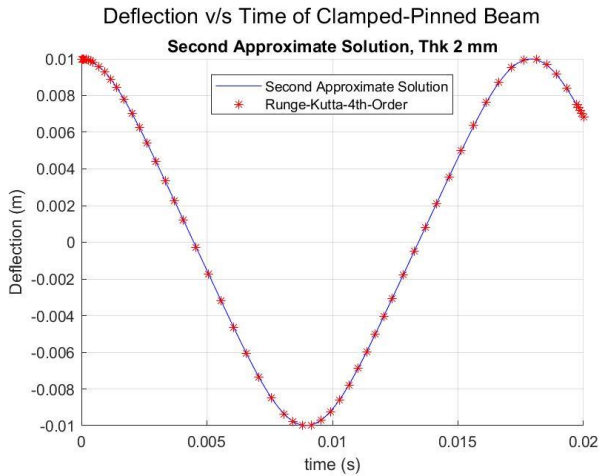


Fig. 18 Mid-point response of 2 mm thick CP beam

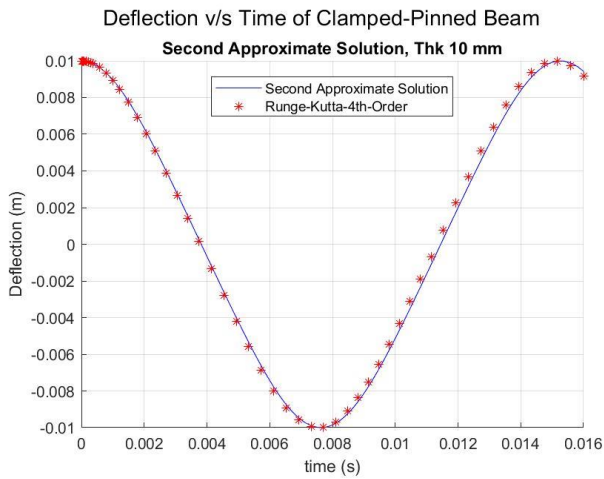


Fig. 19 Mid-point response of 10 mm thick CP beam

The results indicate that the response more closely matches the response from the *RK4* solution for a 2 mm thick beam. Visible variation is found in the case of response from a 10 mm thick beam. It is noted that the second-order approximate method provides an accurate response when strong nonlinearities are present. In contrast, the response is less accurate in the case of moderate nonlinearities. The pattern of response accuracy demonstrated is the reverse of the one observed using the first-order approximate solution.

4.4. Comparison of results by first and second approximate methods

The non-linear frequency by first- and second-order methods for three boundary conditions for 2 mm, 6 mm, and 10 mm thick beams are estimated and compared with an exact non-linear frequency given by Equation 53. The values are tabulated in Table 4. The difference is characterized as an error given by,

$$\% Error = \frac{(\omega - \omega_{ex})}{\omega_{ex}} \times 100 \tag{54}$$

It is noted that the error concerning non-linear frequency estimate for a 2 mm thick beam is of the order of 2.15% and -0.03% with the first approximate solution and second approximate solution, respectively. With a 10 mm thick beam, the error value is 0.91% to 1.1% using the first approximate solution, whereas the error value ranges from -1.12% to -1.67% when the second approximate solution is used. The error percentage order is between the two cases for a 6 mm thick beam. Compared with the exact non-linear frequency, the first-order solution over-predicts the natural frequency, whereas the second-order solution under-predicts the frequency. It is noted that the second approximate method predicts non-linear frequency more accurately than the first approximate method when strong nonlinearity is present. When nonlinearities are moderate, the first approximate method provides relatively more accurate results.

Table 4. Comparison of Non-Linear Frequencies for $A_0 = 10$ mm

Thickness in mm	Boundary Condition	ω in rad/s^2 Exact eq. (53)	ω in rad/s^2 First eq. (42)	% Error eq. (42) v/s eq. (53)	ω in rad/s^2 Second eq. (51)	% Error eq. (51) v/s eq. (53)
2	Pinned-Pinned	213.067	217.624	2.14%	212.997	-0.03%
	Clamped-Clamped	441.703	451.080	2.12%	441.552	-0.03%
	Clamped- Pinned	351.136	358.675	2.15%	351.023	-0.03%
6	Pinned-Pinned	228.623	232.332	1.62%	227.982	-0.28%
	Clamped-Clamped	479.964	487.320	1.53%	478.171	-0.37%
	Clamped- Pinned	374.266	380.524	1.67%	373.382	-0.24%
10	Pinned-Pinned	256.617	259.257	1.03%	253.260	-1.31%
	Clamped-Clamped	547.733	552.716	0.91%	538.572	-1.67%
	Clamped- Pinned	416.256	420.833	1.10%	411.578	-1.12%

Table 5. Comparison of Time Period for $A_0 = 10$ mm

Thickness in mm	Boundary Condition	τ in sec <i>RK4</i>	τ in sec First (43)	% Error (43) v/s <i>RK4</i>	τ in sec Second (50)	% Error (50) v/s <i>RK4</i>
2	Pinned-Pinned	0.02950	0.02887	-2.14%	0.02950	0.00%
	Clamped-Clamped	0.01426	0.013925	-2.35%	0.014235	-0.18%
	Clamped- Pinned	0.01791	0.01752	-2.18%	0.01790	-0.06%
6	Pinned-Pinned	0.02749	0.027045	-1.60%	0.02756	0.25%
	Clamped-Clamped	0.01310	0.01289	-1.60%	0.01314	0.31%
	Clamped- Pinned	0.01681	0.01651	-1.78%	0.01683	0.12%
10	Pinned-Pinned	0.02452	0.02423	-1.16%	0.02480	1.16%
	Clamped-Clamped	0.01148	0.01137	-1.00%	0.01167	1.61%
	Clamped- Pinned	0.01510	0.01493	-1.13%	0.01526	1.06%

Along the same lines, the time period of response is estimated for beam thickness of 2 mm, 6 mm, and 10 mm. The time period is estimated using the first approximate and second approximate solutions for the three boundary conditions and compared with the *RK4* solution. The values are tabulated in Table 5. The difference is characterized as an error given by,

$$\% \text{ Error} = \frac{(\tau - \tau_{RK4})}{\tau_{RK4}} \times 100 \tag{55}$$

The values from Table 5 show that the trend of errors in the time period exhibited is similar to that of non-linear frequency. Using the second approximate solution, the time period estimate matches more closely with the *RK4* solution for a 2 mm thick beam. The first-order solution provides a better estimate of the time period for a 10 mm thick beam. Only in the particular case of the *PP* beam the magnitude of error in the time period is equal in both methods for a 10 mm thick beam. Expectedly, the order of error percentage is between the two cases for a 6 mm thick beam.

4.5. Error v/s NL Frequency Ratio

From the results, it is observed that the magnitude of error varies with the strength of non-linearity. The magnitude of error in frequency as a function of the NL frequency ratio is investigated. The error values for all three boundary conditions and all beam thicknesses from 2 mm to 10 mm are tabulated in Table 6.

Table 6. Error in Non-Linear Frequency Estimate by First and Second Approx. Solutions

Boundary Condition	Thickness in mm	NL Frequency Ratio	% Error eq. (42)	% Error eq. (51)
Pinned-Pinned	2	7.41	2.14%	-0.03%
	4	3.81	1.92%	-0.08%
	6	2.65	1.62%	-0.28%
	8	2.10	1.31%	-0.69%
	10	1.78	1.03%	-1.31%
Clamped-Clamped	2	6.77	2.12%	-0.03%
	4	3.50	1.87%	-0.11%
	6	2.45	1.53%	-0.37%
	8	1.96	1.20%	-0.90%
	10	1.68	0.91%	-1.67%
Clamped-Pinned	2	7.81	2.15%	-0.03%
	4	4.00	1.95%	-0.07%
	6	2.78	1.67%	-0.24%
	8	2.19	1.38%	-0.58%
	10	1.85	1.1%	-1.12%

To understand the behavior of error percentage vis-à-vis NL frequency ratio, the absolute values of error percentage are plotted on the graph for three boundary conditions, as shown in Figures 20, 21, and 22.

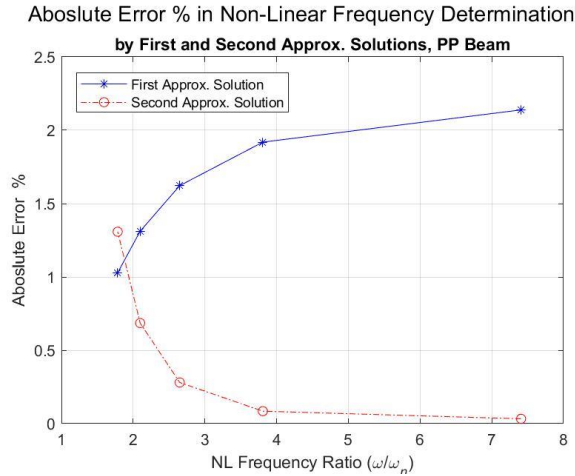


Fig. 20 Absolute % error v/s NL frequency ratio for PP beam

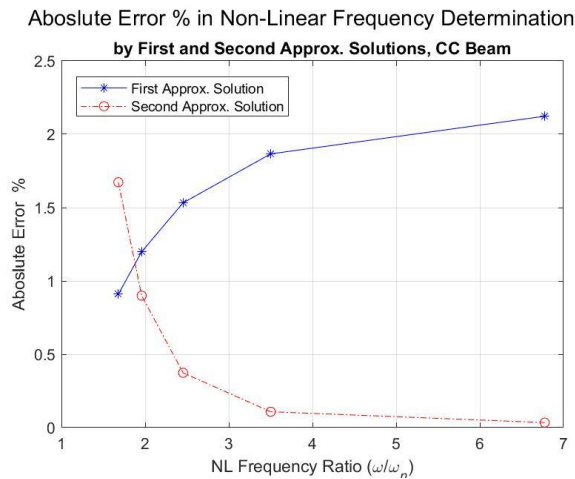


Fig. 21 Absolute % error v/s NL frequency ratio for CC beam

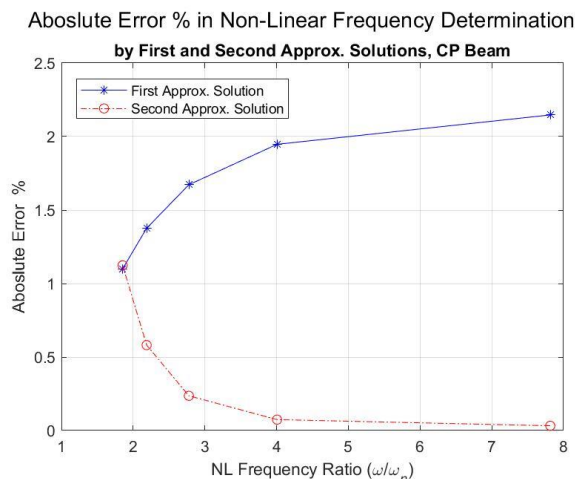


Fig. 22 Absolute % error v/s NL frequency ratio for CP beam

It is observed that the magnitude of error varies with the frequency ratio and appears to follow a discernible trend. The error increases with increasing non-linearity when the first approximate solution is used, whereas the error reduces with increasing non-linearity when the second approximate solution is used. The errors are least for a strongly non-linear beam when the second approximate solution is used. For moderate non-linearity, the first approximate solution provides more accurate results. The behavior of absolute error over frequency ratio tends to follow a non-linear trend. It is observed that both methods appear to have an equal magnitude of the error at one point, and both curves intersect. Authors term this point as a cross-over point. The cross-over point is around the NL frequency ratio of 1.88 for PP and CC beams and 1.76 for CP beams. The value appears to hover around 1.8 for other beam lengths and materials such as aluminum. Research work is still in progress on the cross-over point, and findings will be published subsequently.

5. Conclusion

In the present study, the non-linear free vibration of the beam with pinned-pinned, clamped-clamped, and clamped-pinned boundary conditions are investigated. The first approximate solution with the linear term in α and the second approximate solution with the second-order term in α are used to investigate the accuracy of frequency and response prediction for strong geometric nonlinearity in the beam. The frequencies and response from the two approaches indicate that the second approximate solution predicts the frequency and response more closely with the exact solution and RK4 solution, respectively when strong nonlinearities are present. When non-linearities are moderate, the first approximate solution predicts the response more closely with the RK4 solution. The magnitude of error of non-linear frequency estimate compared to exact frequency is investigated. It is observed that the magnitude of error varies non-linearly as a function of the NL frequency ratio. A cross-over point exists where the magnitude of error between the first and second approximate solutions is the same. In future work, a generalized investigation of prediction accuracy with an expanded range of NL frequency ratios and different materials can be taken up for further investigation. The study may be extended to perform a regression analysis to quantitatively relate the absolute error percentage with the NL frequency ratio.

References

- [1] David Wagg, Simon Neild, Nonlinear Vibration with Control for Flexible and Adaptive Structures, Second Edition, Springer International Publishing Switzerland. (2015) 292-298.
- [2] S. R. R. Pillai and B. Nageswara Rao, On Non-Linear Free Vibrations of Simply Supported Uniform Beams, Journal of Sound and Vibration 159(3) (1992) 527-531.
- [3] W. Lestari and S. Hanagud, Non-Linear Vibration of Buckled Beams: Some Exact Solutions, International Journal of Solids and Structures. 38 (2001) 4741-4757.
- [4] M.T. Ahmadian, M. Mojahedi and H. Moeenfar, Free Vibration Analysis of a Non-Linear Beam Using Homotopy and Modified Lindstedt-Poincare Methods, Journal of Solid Mechanics. 1 (2009) 29-36.
- [5] Jian-She Peng, Yan Liu, and Jie Yang, A Semi-Analytical Method For Non-Linear Vibration of Euler-Bernoulli Beams with General Boundary Conditions, Hindawi Publishing Corporation, Mathematical Problems in Engineering. 591786 (2010) 17.
- [6] Ma Xinmou, Chang Liezhen, and Pan Yutian, Accurate Solutions to Non-Linear Vibration of Cantilever Beam via Homotopy Perturbation Method, Procedia Engineering. 15 (2011) 4768-4773.
- [7] Hamid M. Sedighi, Kourosh H. Shirazi, A and Noghrehabadi, Application of Recent Powerful Analytical Approaches on the Non-Linear Vibration of Cantilever Beams, International Journal of Nonlinear Sciences and Numerical Simulation. 13(7-8) (2012) 487-494.
- [8] A.Barari, H.D. Kaliji, M. Ghadimi, and G. Domairry, Non-Linear Vibration of Euler-Bernoulli Beams, Latin American Journal of Solids and Structures. 8 (2011) 139-148.
- [9] Debabrata Das, Prasanta Sahoo, and Kashinath Saha, A Numerical Analysis of Large Amplitude Beam Vibration Under Different Boundary Conditions and Excitation Patterns, Journal of Vibration and Control. 18(12) (2012) 1900-1915.
- [10] S.S. Jafari, M.M. Rashidi, and S. Johnson, Analytical Approximation of Non-Linear Vibration of Euler-Bernoulli Beams, Latin American Journal of Solids and Structures. 13 (2016) 1250-1264.
- [11] S. Bagheri, A. Nikkar and H. Ghaffarzadeh, Study of Non-Linear Vibration of Euler-Bernoulli Beams Using Approximate Analytical Techniques, Latin American Journal of Solids and Structures. 11 (2014) 157-168.
- [12] Iman Pakar and Mahmoud Bayat, Analytical Study on the Non-Linear Vibration of Euler-Bernoulli Beams, Journal of Vibro Engineering. 14(1) (2012).
- [13] Mohammadreza Azimi and Saeed Kariman, Periodic Solution for Vibration of Euler-Bernoulli Beam Subjected to Axial Load Using DTM and HA, Journal of Applied Mechanical Engineering. 2(2) (2013) 1000125.
- [14] A.A. Motallebi, M. Poorjamshidian, and J. Sheikhi, Vibration Analysis of a Nonlinear Beam under Axial Force by Homotopy Analysis Method, Journal of Solid Mechanics. 6(3) (2014) 289-298.
- [15] O. Barry, Non-Linear Vibration of an Axially Loaded Beam Carrying Rigid Bodies, AIP Advances. 6(12) (2016).
- [16] Shahin Mohammadrezazadeh, Ali-Asghar Jafari and Mohammad Saeid Jafari, An Analytical Approach for the Non-Linear Forced Vibration of the Clamped-Clamped Buckled Beam, Journal of Theoretical and Applied Vibration and Acoustics. 3(2) (2017) 127-144.
- [17] Hu Ding, Yi Li and Li-Qun Chen, Non-Linear Vibration of a Beam with Asymmetric Elastic Supports, Nonlinear Dynamics. 95 (2019) 2543-2554.
- [18] Van - Hieu Dang and Quang- Duy Le, Analysis of Nonlinear Vibration of Euler-Bernoulli Beams Subjected to Compressive Axial Force via the Equivalent Linearization Method with a Weighted Averaging, International Journal of Scientific and Innovative Mathematical Research. 7(1) (2019) 4-13.
- [19] Tobias Friis, Marius Tarpø, Evangelos I. Katsanos and Rune Brincker, Equivalent Linear Systems of Nonlinear Systems, Journal of Sound and Vibration. 469 (2020).
- [20] Mahmoud Bayat, Iman Pakar, and Paul Ziehl, Nonlinear Vibration of Axially Loaded Railway Track Systems Using Analytical Approach, Journal of Low-Frequency Noise, Vibration and Active Control. 0(0) (2021) 1-11.
- [21] A. Rincón-Casado, J. González-Carbajal, D. García-Vallejo and J. Domínguez, Analytical and Numerical Study of the Influence of Different Support Types in the Non-Linear Vibrations of Beams, European Journal of Mechanics / A Solids. 85 (2021) 104113.
- [22] Ehsan Loghman, Firooz Bakhtiari-Nejad, Ali Kamali E, Mostafa Abbaszadeh and Marco Amabili, Non-Linear Vibration of Fractional Viscoelastic Micro-Beams, International Journal of Non-Linear Mechanics. 137 (2021) 103811.
- [23] Omar Outassafte, Ahmed Adri, Yassine El Khouddar, Said Rifai and Rhali Benamar, Geometrically Non-Linear Free In-Plane Vibration of Circular Arch Elastically Restrained Against Rotation at the Two Ends, International Journal of Engineering Trends and Technology. 69(3) (2021) 85-95.
- [24] Walter Lacarbonara and Hiroshi Yabuno, Refined Models of Elastic Beams Undergoing Large In-Plane Motions: Theory and Experiment, International Journal of Solids and Structures. 43 (2006) 5066-5084
- [25] H. Hu, A Classical Perturbation Technique Valid for Large Parameters, Journal of Sound and Vibration. 269 (2004) 409-412.
- [26] Singiresu S. Rao, Vibration of Continuous Systems, John Wiley & Sons, Inc., Hoboken, New Jersey. (2007) 326-334
- [27] Robert D. Blevins, Formulas for Dynamics, Acoustics and Vibration, First Edition, John Wiley & Sons, Ltd. (2016) 429-434.